Acta Astronautica 237 (2025) 409–420

Contents lists available at ScienceDirect

Acta Astronautica

journal homepage: www.elsevier.com/locate/actaastro

3D printing LDPE/lunar regolith simulant composite: manufacturing with in-situ resources on the moon

S. Moazen [a], F.P. Gosselin [b], I. Tabiai [a], M. Dubé [a,*]

[a] CREPEC, Department of Mechanical Engineering, École de technologie Supérieure, Montréal, Québec, Canada
[b] CREPEC, Polytechnique Montréal, Montréal, Québec, Canada

ARTICLE INFO

Keywords:
3D printing
In-situ resource utilization
In-space manufacturing
Lunar regolith
Packaging grade LDPE

ABSTRACT

Additive manufacturing is essential for space missions, enabling on-demand production of components where resupply from Earth is limited. Fused deposition modeling (FDM) offers a promising route for repurposing plastic packaging waste into 3D printing feedstock. Low-density polyethylene (LDPE), commonly used in space packaging, can be combined with lunar regolith simulant to increase material availability for in-situ resource utilization (ISRU). However, the method of incorporating regolith into the polymer matrix affects filament quality and printability. Here, we compare single-screw and twin-screw extrusion techniques for producing LDPE/regolith composite filaments containing up to 30 wt% regolith. Both methods successfully produced filaments suitable for FDM, though single-screw extrusion required a second extrusion step above 10 wt% regolith. Filaments were evaluated for diameter consistency and printability, including the successful fabrication of NASA-designed parts. Regolith addition enhances print performance by improving overhang formation, gap bridging, and reducing warpage. Tensile testing shows increased stiffness without compromising strength up to 20 wt% regolith. These results demonstrate that LDPE and lunar regolith can be effectively processed into printable feedstock, supporting sustainable manufacturing strategies for lunar applications and advancing terrestrial plastic waste recycling.

1. Introduction

Additive manufacturing (AM) is a key technology for space exploration as it offers unparalleled flexibility by enabling on-demand production of customized parts, which is particularly critical in space environments where immediate access to Earth made components is not possible [1,2]. Moreover, it supports in-situ resource utilization (ISRU), where local materials such as lunar regolith can be used to fabricate tools, components, or structures directly at the exploration site, minimizing the launch mass and costs. Beyond regolith, mission waste -particularly plastic packaging-offers another valuable resource for AM, addressing both material shortages and waste management challenges.

Waste management remains a critical challenge for long-term crewed missions, as current practices, such as compacting waste and incinerating it upon re-entry to atmosphere, are unsustainable. NASA's model estimates that food and packaging waste will constitute the second-largest proportion of total waste generated, behind only human waste [3]. Various AM methods have been explored for ISRU, with several review studies detailing their potential applications [4–10]. Among these methods, fused filament fabrication (FFF) is particularly promising for repurposing plastic waste into printable feedstock and was the first AM technique demonstrated to function in space. Since then, other methods, such as metal wire arc additive manufacturing (WAAM) and ceramic stereolithography (SLA) have also been tested on ISS [11, 12]. The "In-Space Manufacturing" project has confirmed that parts 3D printed in microgravity using FFF are comparable to those produced on Earth [1,13,14].

Despite the technology's potential, studies on FFF 3D printing of polymer/regolith composites are few. Adding regolith, a virtually unlimited resource on the moon, to polymer is an obvious way to increase ISRU and print more parts with a given amount of Earth-originating material, but it affects the printed part mechanical properties. Li et al. [15] fabricated filaments of PLA and ball milled CLRS-1 lunar regolith simulant with an average size of 2.5 μm using a Parallel 11 twin screw extruder at 5 and 10 wt% regolith. They reported that tensile strength decreases with the addition of regolith, which was attributed to the increased porosity of the printed parts. In the same vein, Zaccardi et al. [16] mixed medium density polyethylene with 5 and 10 wt% of Martian

* Corresponding author.
E-mail address: martine.dube@etsmtl.ca (M. Dubé).

https://doi.org/10.1016/j.actaastro.2025.08.012
Received 28 April 2025; Received in revised form 22 July 2025; Accepted 4 August 2025
Available online 2 September 2025

regolith simulant into a filament for FFF 3D printing. Basalt powder with an average diameter of below 45 μm was used as Martian regolith simulant. A FilaFab single screw filament maker extruded the composite filaments. Clogging is a common challenge for 3D printing of particulate-filled polymer composites, and to avoid that, no more than 10 wt% of regolith was added to the PE and a 0.8 mm nozzle was used instead of the standard 0.4 mm nozzle. A decrease in tensile properties upon addition of regolith was attributed to the irregular shapes of the particles, which act as stress concentrators [16].

To limit the dependency on Earth, using higher percentage of regolith is favorable. Azami et al. incorporated 30 wt% regolith into PEEK using a parallel 11 twin-screw extruder. The composite exhibited reductions of 26.8 % in tensile strength and 62 % in elongation at break due to increased porosity in the sample [17]. In a 2024 report by NASA, PLA/regolith composites containing up to 80 % regolith were printed. They employed a fused granular fabrication (FGF) method, in which the feedstock is in pellet form. Depending on the model of 3D printer, the nozzle diameter of FGF printers can be much larger than for FFF 3D printers, which enables the possibility to print at higher regolith content, as the chances of clogging are reduced. A nozzle with a diameter of 3 mm was used in this case [18]. One of the important factors that should be considered for space applications is outgassing. Outgassing occurs in some materials when they're exposed to the vacuum condition of space. In this regard, PLA is not a space grade material [19]. Furthermore, using PEEK or PLA would require bringing them to the mission. This added weight increases launch costs and logistical challenges, making them less practical for resource utilization in space.

Low-density polyethylene (LDPE), commonly used for the packaging of goods taken during missions, has the potential to be repurposed for 3D printing applications [2,20]. However, the 3D printing of LDPE is not extensively investigated and is in its early stages of development. Three primary challenges hinder its use in additive manufacturing: filament buckling, bed adhesion, and volume shrinkage upon cooling.

Filament buckling between the extruder and the nozzle during printing has been reported in various studies, primarily attributed to LDPE's low modulus, which is typically of the order of 0.1–0.3 GPa [21]. The filament needs to have sufficient stiffness to resist compressive forces from the extruder; otherwise, it can deform and buckle, leading to improper feeding into the nozzle and potential print failures. This limitation restricts printing speed, as the required pressure drop to extrude the filament increases with the flow rate (printing speed) [22,23]. Consequently, reported printing speed did not exceed 4 mm/s [22–24]. To address this issue, Olesik et al. [25] incorporated 15 and 30 vol% powdered waste glass particles, enhancing the modulus by 8 % and 13 %, respectively, and thereby increasing the maximum achievable printing speed without inducing buckling. As a result, the printing speed increased slightly from 2.38 mm/s to 2.75 mm/s and 2.95 mm/s for 15 vol% and 30 vol% glass content, respectively.

Viscosity is another critical factor influencing buckling behaviour. According to Venkataraman et al., the ratio of modulus to viscosity (E/η) must exceed a critical threshold to avoid buckling [27]. This suggests that, at a given modulus, a polymer with lower viscosity is less prone to buckling and can achieve higher flow rates and printing speed. The melt flow index (MFI) is a widely recognized rheological property influencing the suitability of polymers for 3D printing. A recommended MFI of approximately 10 g/10 min has been proposed for FFF 3D printing [28–30]. For instance, Bedi et al. reported printing LDPE composites containing 50 wt% Al_2O_3 with an MFI of 10.53 g/10 min at speeds up to 60 mm/s [29], demonstrating that achieving higher printing speeds is feasible when LDPE exhibits lower viscosity.

Poor adhesion to common print beds is a challenge for LDPE printing. This issue can be mitigated by using alternative bed materials that improve adhesion. A variety of bed materials have been tested, and among them, HDPE, SEBS, Kapton tape, roughened HDPE, blue painter's tape, and combinations of Kapton tape with Elmer's glue stick have been used for successful printing [26,31–33].

Significant volume shrinkage during crystallization and solidification of LDPE, exacerbating warping, makes its printing challenging. In addition to the inherent warpage caused by the layer-by-layer nature of 3D printing, PE's high degree of crystallinity results in severe shrinkage upon cooling, making the material particularly prone to warping. To address this issue, strategies such as blending PE with other polymers or incorporating fillers to create composites have been employed [34,35]. Filament fabrication involves melt mixing of polymers with particles, where the choice of fabrication and mixing method plays a crucial role in the dispersion and distribution of particles within the polymer matrix. Both single-screw and twin-screw extruders are commonly used for incorporating particles into polymer feedstock for FDM [36–38]. Twin-screw extruders are known for their superior mixing capabilities, while single-screw extruders offer advantages such as lower cost, simpler design, and reduced power consumption [11,12]. The choice of extruder for lunar applications may vary based on factors such as energy efficiency, cost, particle weight percentage, and application-specific requirements. However, there remains a need to systematically investigate how the use of single screw versus twin screw extruders affects the printability of the filament and the properties of the fabricated parts.

The definition of printability has been a longstanding focus for researchers [39–41]. For a material to be considered printable, it must meet some essential criteria: (1) it must be extrudable through a nozzle, (2) maintain its shape after extrusion, (3) retain geometric stability as it cools to ambient temperature, (4) have the capacity to bridge gaps, and (5) should be capable of producing small features defined as below 10 mm [42–44].

Here, we present a comparative analysis of single screw and twin screw extrusion methods for producing highly printable composite filaments made of packaging grade LDPE and lunar regolith simulant. The printability of the filaments is evaluated by assessing filament diameter consistency and printing various parts, including torture part and NASA-designed components, while tensile testing investigates the effects of regolith content and extrusion method on mechanical properties. This study demonstrates how the choice of polymer grade, extrusion technique, and regolith content influence filament uniformity, printability, and mechanical performance which can be applied in both terrestrial and space-based manufacturing applications.

2. Materials and methods

2.1. Materials

Two different packaging grades of LDPE, in virgin form, were used in this study. First, an LDPE with a melt flow index of 0.9 g/10 min (190/2.16) and density of 0.922 g/cm^3 was supplied by Marplex in powder form. The second polymer was sourced as LDPE (DOW™ 722) pellets, from DOW chemicals with a melt flow index of 8 g/10 min (190/2.16) and a density of 0.918 g/cm^3. Marplex and DOW LDPE are referred to as m-LDPE and d-LDPE, respectively.

Lunar mare regolith simulant (LMS-1D), a commercially available mineral-based material designed to replicate the average composition of mare-type lunar soil, was sourced from SpaceResourceTech (former ExolithLab). Detailed information on its chemical composition and particle size distribution is provided in Tables S1 and S2 of the Supporting Document, alongside comparisons with the JSC-1 simulant and regolith samples from the Apollo missions. LMS-1D has a particle size range of 0.04–35 μm, with a mean size of 6 μm. This size distribution was selected over one that more closely resembles Apollo regolith, as it is better suited for FFF 3D printing and can be used as received, eliminating the need for additional milling, which is typically required to avoid nozzle clogging when larger particles are present. An SEM image of the particles is shown in Fig. S1 (see Supporting Document).

While future lunar missions are planned to be close to the lunar South Pole, which is rich in highland regolith, here we selected LMS-1D, a mare regolith simulant. The choice was primarily based on practical

considerations: highland simulants generally have higher hardness, which can increase damage to extrusion systems. Using compositional data and the rule of mixtures, the Mohs hardness of LMS and a representative highland simulant available to us (Chenobi) were estimated to be approximately 6.2 and 7, respectively. Since the simulant in this study functions mainly as a filler in the polymer matrix, the difference in mineralogy between mare and highland regolith is not expected to significantly impact the material's printability or behaviour during processing. This choice represents a limitation in terms of site-specific fidelity, but it was considered acceptable within the scope of this work.

2.2. Filament fabrication

Two different machines were used for filament fabrication. The first one is a desktop filament extruder (3Devo, Netherlands). This machine is equipped with a single screw extruder with four different heating zones, two fans acting as a cooling system, two rollers to pull the filament, an optical sensor for measuring the filament diameter with a 43 μm precision and a spooling system. The second machine is a Process 11 Parallel twin screw extruder. As the extruded filament leaves the die, it is cooled using compressed air jets and then spooled using Felfil spooler+, with a diameter sensor accuracy of 10 μm.

Filaments of both grades of LDPE were fabricated by the 3Devo filament extruder and initially evaluated for their suitability for 3D printing. Based on these preliminary assessments, d-LDPE was selected for composite fabrication. To improve the homogeneity of regolith distribution, filaments were produced using either a single or double extrusion process. The double-extruded filaments were generated by re-extruding the pelletized, once-extruded filaments. The resulting filaments are referred to as SSX-Y and TSX-Y, where SS, TS, X and, Y stand for single screw extrusion, twin screw extrusion, number of extrusions, and regolith wt%, respectively. Fig. 1 shows a schematic of the filament fabrication process.

To provide better mixing with regolith, d-LDPE pellets were pulverized into powder form. Prior to extrusion, polymer and regolith were dried overnight at 65 °C. Next, LDPE and regolith (up to 30 wt%) were manually mixed in a jar for at least 4–5 min before being fed to the extruder. Extrusion parameters for each filament were obtained through different trials, aiming to achieve consistency in filament diameter and proper surface quality by visual inspection. Detailed processing parameters are listed in Table S3 (see Supporting Document).

The 3Devo filament extruder is equipped with a software that enables real-time monitoring of filament diameter, providing data to evaluate filament uniformity along its length. Filament diameter was recorded at an acquisition rate of 1 Hz over lengths of 100 m and 230 m for SS1 and SS2 filaments, respectively. The data was analyzed to determine the diameter distribution using kernel density estimation. Additionally, the frequency of occurrences within specified diameter ranges was calculated using a Python script and reported as percentages in Table S4 (see Supporting Document). The TS1 setup did not include this feature. Therefore, TS1 filaments were manually checked for diameter consistency and surface irregularities by passing them through a 1.9 mm internal diameter tube.

2.3. X-ray microtomography

X-ray microtomography (μ-CT) was employed to observe the distribution of regolith simulant particles in the filament, particularly those with repeating surface irregularities. The scan of surface irregularity was performed using a Nikon XTH 225. To achieve higher resolution and better capture the fine regolith particles, additional scans were carried out using an Xradia 520 Versa device (Zeiss, Canada), operated at 60 kV acceleration voltage, 5 W power, with a 4 × objective, and 10 s exposure time per scan. This system provided a voxel size of 2.19 μm, compared to the 15 μm resolution of the Nikon system. The higher-resolution scans were used to analyze SS2 filaments. Image reconstruction was done using Dragonfly software (Object Research Systems, Canada).

2.4. 3D printing

3D printing was performed using an Ender-5 S1 3D printer. The printability of the filaments was evaluated by printing in vase mode as well as printing a 3D Benchy in default mode. Rectangular cuboids (100 × 8 × 4 mm) were printed to evaluate warpage. Tensile test samples were printed according to the ASTM D638 Type IV standard. The dimensions are now included in Fig. 2a, which presents a 3D schematic of the sample. The X–Y plane corresponds to the printing bed, while the sample thickness is built along the Z-axis. Each sample includes an outer perimeter wall and a cross-ply infill pattern with alternating layers oriented at 0° and 90°. For clarity, the 90° layer is only partially shown to expose the underlying 0° layer. Fig. 2b presents a 2D cross-sectional view of the gauge section, illustrating the internal infill structure and the relationship between the printing direction and principal stress during tensile testing (aligned along the X-axis).

NASA previously designed and printed various mission accessories and functional tools as part of in-space manufacturing project [45] to showcase on-demand production. To demonstrate the applicability of the LDPE/regolith composite developed here, we printed the same parts using the composite filament containing 30 wt% regolith. The CAD files for these parts were sourced from NASA's publicly available database to ensure consistency in design [46]. A 2.4 mm thick brim was added to the first layer of all samples to enhance bed adhesion. Printing parameters were calibrated to ensure good visual quality. Key parameters are listed in Table 1. To avoid nozzle clogging and ensure consistent print quality, the nozzle was purged with pure polymer and cleaned using the.

cold pull technique between prints to remove residual material. Due

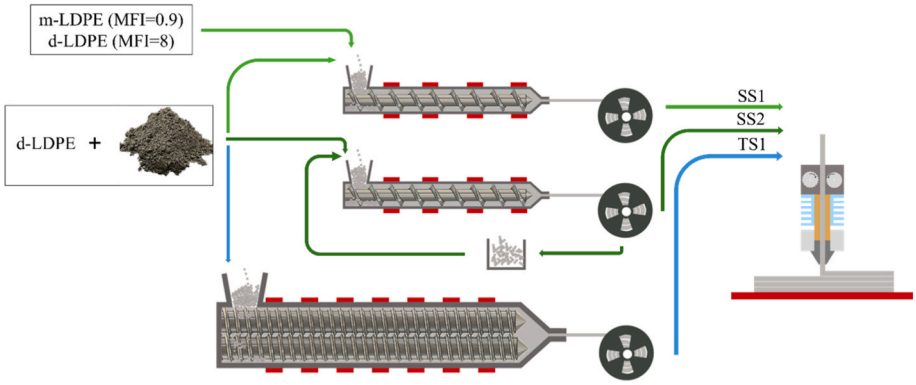

Fig. 1. Schematic of the three filament fabrication processes considered: one-pass single screw extruder (SS1); twice-extruded single screw extruder (SS2); and one-pass twin screw extruder (TS1).

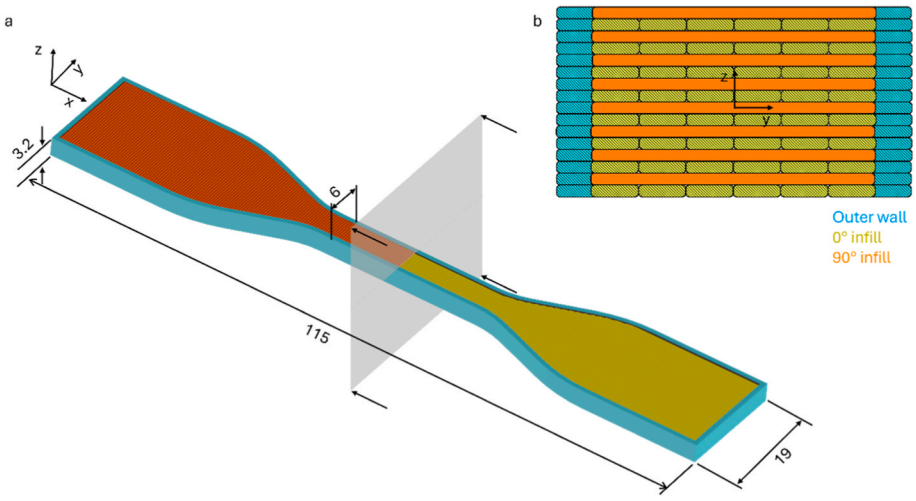

Fig. 2. Schematic and infill pattern of tensile samples: a) 3D schematic representation showing dimensions and geometry of the ASTM D638 type IV tensile sample, with a highlighted sectioning plane intersecting the gauge region; and b) 2D cross-sectional view illustrating the alternating 0°–90° cross-ply infill pattern.

Table 1
3D printing parameters.

Sample	Nozzle diameter (mm)	Nozzle temperature (°C)	Bed temperature (°C)	Printing speed (mm/s)	Layer height (mm)	Print Infill (%)
Vase (m-LDPE)	0.8	235	60	2, 4	0.32	N/A
Vase (d-LDPE and composites)	0.4, 0.6, 0.8	210	60	20	0.32	N/A
3D Benchy	0.8	210	60	20	0.32	20
Warpage, Tools	0.8	210	60	20	0.32	100
Tensile	0.8	210	60	20	0.2	100

to the abrasive nature of regolith, a MicroSwiss M2 hardened steel nozzle was employed to improve durability and prevent clogging. To ensure that filament diameters ≥1.9 mm did not interfere with the extrusion process, the filaments were passed through a heat break prior to printing to confirm that only filaments with diameters within the suitable range were used for printing.

Six different bed materials, including Creality's glass and ultra-flexible magnetic beds, PEI and BuildTak™ sheets (McMaster-Carr), polyimide tape, and SEBS film (Vreebreg, Netherlands), were tested for adhesion of the initial printed layer. When adhesion was inadequate, Elmer's all-purpose glue stick and a nano-polymer adhesive (Vision Miner) were applied to the bed surfaces to evaluate their ability to enhance adhesion. In total, 16 different configurations were tested.

2.5. 3D scan

Dimensional accuracy and geometric deviations of 3D Benchy models and vases printed with pure LDPE and composite filaments were evaluated by scanning the parts using a Hexagon Absolute Arm 3D scanner. The scanned point cloud data were processed in PolyWorks Inspector™, where each part was aligned to its corresponding CAD model using pre-alignment with paired points, followed by best-fit alignment. Surface deviation maps and statistical data, including the mean and standard deviation of dimensional errors, were generated to assess the geometric fidelity of the printed parts.

To visualize the distribution of dimensional deviations, probability density function (PDF) curves were generated using the normal distribution equation:

$$f(x) = \frac{1}{\sigma\sqrt{2\pi}} \times e^{-\frac{(x-\mu)^2}{2\sigma^2}}$$

where μ is the mean deviation and σ is the standard deviation. The variable x, representing the deviation from the CAD model, was evaluated over a range of −3 mm to +3 mm ensuring that the full span of $\pm 3\sigma$ for both materials.

2.6. Tensile testing

Tensile tests were performed using an MTS Insight Electromechanical testing machine according to the ASTM D638-type IV standard. Five samples were tested for each material. An MTS DX 2000 High Strain Extensometer equipped with a rubber knife edge was used for strain measurements. The tests were conducted at a crosshead speed of 50 mm/min, corresponding to approximately 30 mm/min in the gauge length. Stress was calculated by dividing the load by the average of 5 original cross-sectional area measures in the gage length.

3. Results and discussion

3.1. Filament fabrication

Maintaining a consistent filament diameter is critical for ensuring stable material feed during 3D printing. The standard filament diameter tolerance reported in the literature is 1.75 ± 0.05 mm, with an acceptable expanded tolerance range of 1.75 ± 0.1 mm [47]. Deviations beyond this range, such as diameters below 1.65 mm or above 1.85 mm, can result in extrusion failure. Specifically, filaments that are too small may not be adequately gripped by the extruder's gears, while those exceeding 1.85 mm may fail to pass through the heatbreak. However, the thresholds can vary depending on printer specifications. Here, the heatbreak inner diameter was 1.9 mm, allowing diameters up to this value to pass through. Despite being outside the literature's acceptable limits, diameters in the range of 1.85–1.9 mm and below 1.65 mm did not impede extrusion. The smallest recorded diameter was 1.6 mm, and the suitable range for reliable extrusion was thus extended to 1.75 ± 0.15 mm.

During the fabrication of filaments with 20 wt% and 30 wt% regolith using the single-screw extruder (SS1), diameters exceeding 1.9 mm were

more frequent. Visual inspection revealed the presence of surface irregularities, or "bumps" (Fig. 3a), which caused the diameter to exceed the suitable range. As shown in Fig. 3b, these bumps can disrupt the extrusion. As can be seen in Fig. 3c, X-ray microtomography showed that the bumps corresponded to clusters of regolith near the filament surface. This clustering likely arises from the limited mixing capability of the single-screw extruder, which lacks the shear forces required for the effective dispersion of high regolith content within the polymer matrix. To further illustrate the regolith distribution, representative μ-CT cross-sections of SS2-10, SS2-20, and SS2-30 filaments are included in the Supporting Document (Fig. S2).

To evaluate diameter variations, recorded data from the 3Devo sensor were analyzed. The distribution of filament diameters was visualized using kernel density estimation (KDE), as shown in Fig. 3d–g. The KDE curves represent the probability density of filament diameters. Additionally, the percentage occurrence within specific diameter ranges is summarized in Table.

S2 (Supporting Document). As can be seen in Fig. 3d, for pure LDPE filaments, 100 % of the measured diameters fall within the suitable range. However, as the regolith content increases in SS1 filaments in Fig. 3e–g, the Gaussian fit over the KDE curve becomes wider, indicating significant diameter variability at 20 wt% and 30 wt% regolith. In contrast, twice extruded filaments (SS2) show improved consistency. The second extrusion process acts as an additional melt-mixing step, where shear forces during extrusion break up the regolith clusters and improve their dispersion in the polymer matrix. This effect is evident in the plots, where the Gaussian fit at 30 wt% regolith is more centered around 1.75 mm with significantly fewer diameters exceeding the suitable range.

The frequency of surface clusters is critical because the length of the filament spanning two consecutive clusters is useable for 3D printing. High cluster frequency can result in short filament segments, insufficient for completing a print. Fig. 4 illustrates the distribution of useable filament lengths produced under different conditions. The box represents the interquartile range (IQR), where the middle 50 % of the data lie. The horizontal line inside the box shows the median filament length. The whiskers extend to the smallest and largest values within 1.5 times the IQR. Points outside the whiskers are considered outliers and the hollow black square shows mean value. As can be seen, filaments produced with SS2 have longer and more uniform lengths compared to those from SS1, which can be attributed to the reduction in surface clusters, consistent with KDE plots.

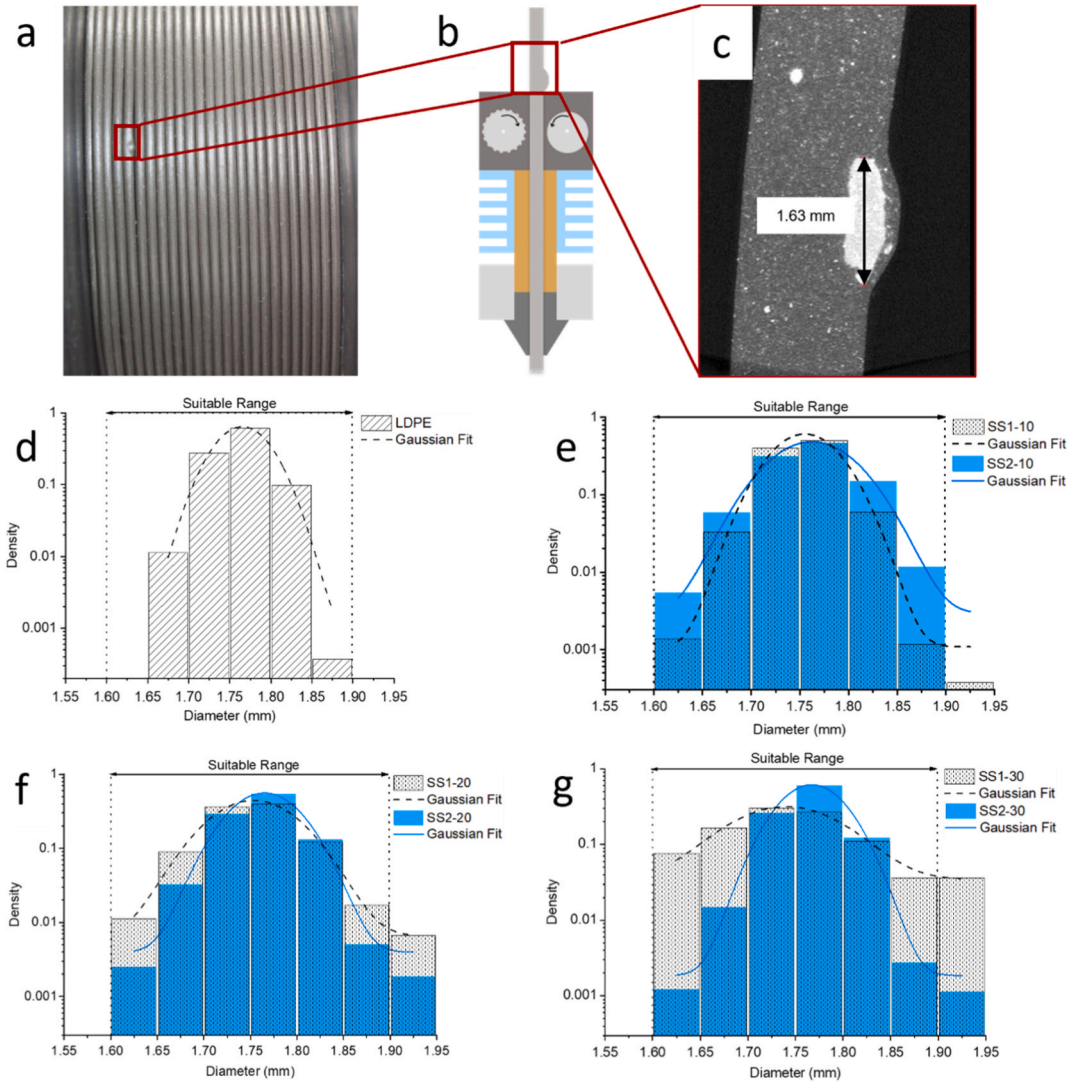

Fig. 3. Regolith cluster effects on filament extrusion and diameter consistency: a) filament image showing a surface irregularity (regolith cluster); b) schematic of extrusion failure caused by clusters; c) micro-CT image confirming the formation of regolith cluster; d-h) KDE plots of filament diameters for one (SS1), and two (SS2) extrusions at different regolith contents.
Re-extrusion reduces diameter variability and improves filament consistency.

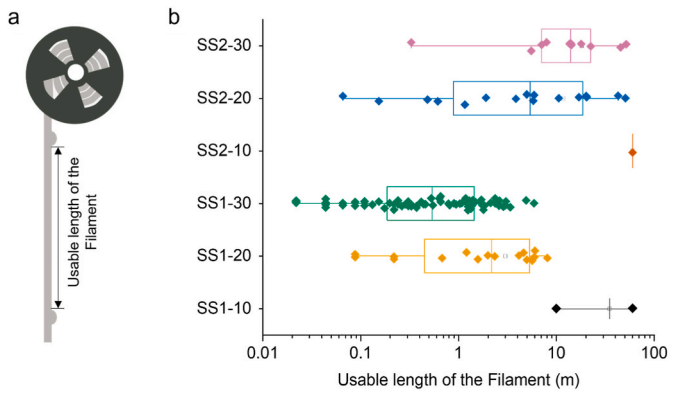

Fig. 4. Filament length spanning two consecutive out-of-spec diameter values: a) schematics of the defined useable length of filament between two consecutive out-of-spec diameter values; and b) box plots of the defined length produced by different methods and regolith wt%. SS2 filaments are longer and more uniform, showing that re-extrusion reduces clusters and improves consistency, especially at higher regolith contents.

At 10 wt% regolith, SS1 filaments contain only one surface cluster, yielding relatively long printable filament segments. After re-extrusion, no surface clusters are observed, resulting in a continuous filament length of approximately 100 m within the suitable diameter range. At 20 wt% and especially 30 wt%, SS1 filaments exhibit high variability in printable filament lengths. While some outliers at higher lengths indicate occasional success, the overall inconsistency suggests significant challenges in achieving long suitable filaments. In contrast, SS2 filaments showed substantial improvement, with reduced length variability and longer, stable segments. This demonstrates that the second extrusion process is effective in mitigating clustering, making it a suitable approach for producing long, consistent filaments for 3D printing at higher content.

Notably, no surface clusters were observed on the TS1-20 and TS1-30 filaments, likely due to the higher shear forces applied by the twin-screw extruder, which improves the dispersion of the regolith in the polymer matrix.

3.2. 3D printing

To assess the adhesion of the extruded filament to the print bed, 16 different configurations were evaluated. Among these, SEBS sheets consistently demonstrated reliable performance. Although the BuildTak™ sheet initially provided adequate adhesion, the printed parts detached after the first layer, resulting in print failure. In contrast, SEBS sheets maintained a strong and consistent bond throughout the printing process, effectively resisting forces generated by warpage.

The printability of the fabricated filaments was evaluated using two modes: vase mode and default mode. Extrudability, defined as the ability of a material to pass through the nozzle without interruptions, is the primary prerequisite for achieving printability. This property becomes particularly critical when particles are introduced into a polymer matrix, as they can increase the likelihood of nozzle clogging. Consistent material flow, a key aspect of extrudability, was assessed using printing in vase mode, also known as “spiralize outer contour” mode. This method involves printing a continuous, single-wall structure in a spiral without retractions or layer changes, making it ideal for identifying flow inconsistencies, irregular extrusion, or clogging during 3D printing.

Printing vases with low melt flow index LDPE was not feasible. The low MFI value (0.9 g/10 min) caused difficulties in extrusion and inconsistencies in filament deposition, making it impossible to print even at a low speed of 2 mm/s (Fig. S3). In contrast, as shown in Fig. 5a, LDPE with an MFI of 8 g/10 min was successfully printed at a speed of 20 mm/s, exhibiting consistent flow and extrudability. This underscores the significance of MFI in determining the suitability of waste materials for repurposing as 3D printing feedstock.

Fig. 5b–d presents vases printed with different regolith content. All samples show a good overall print quality and surface finish. Additional images of the scanned vases, including their deviation map are provided in Supporting Document (Fig. S4). Table 2 summarizes the success or failure of the printed vase using composite filaments with different nozzle sizes. SS2 and TS1 filaments demonstrated consistent material flow with nozzle diameters of 0.6 mm and 0.8 mm, whereas SS1 filaments were extrudable only at a regolith content of 10 wt%. These

Table 2
Vase printability using different nozzle sizes and filament extrusion methods.

Extrusion Process	Regolith wt %	Nozzle Diameter (mm)		
		0.4	0.6	0.8
SS1	10	×	×	✓
	20	×	×	×
	30	×	×	×
SS2	10	✓	✓	✓
	20	×	✓	✓
	30	×	✓	✓
TS	20	×	✓	✓
	30	×	✓	✓

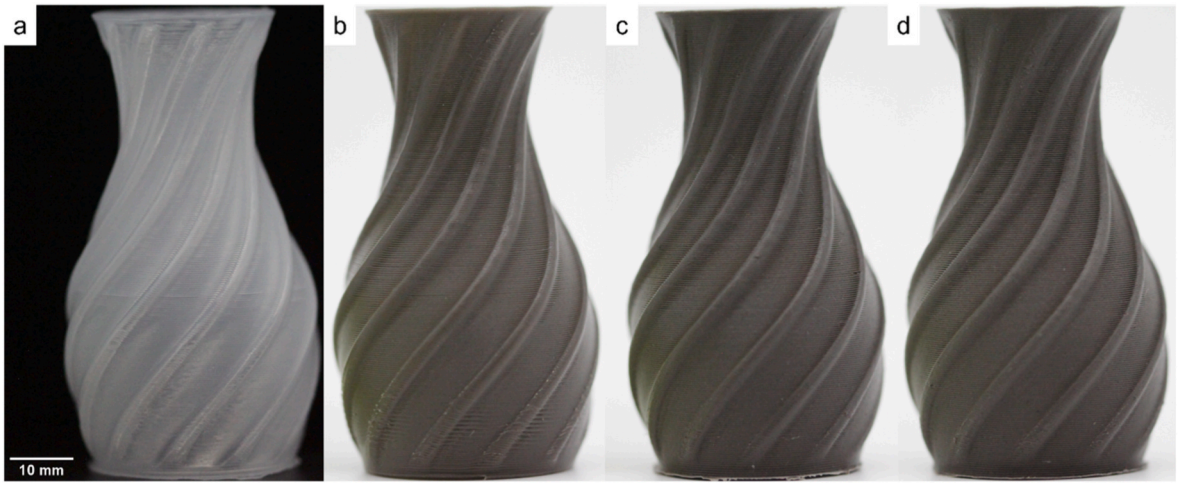

Fig. 5. 3D printed vases using different materials. a) pure d-LDPE, and its composites containing b) 10 wt%, c) 20 wt%, and d) 30 % wt regolith. The developed composites demonstrate good extrudability by printing in vase mode.

results show that to avoid nozzle clogging and maintain extrudability with more than 10 wt% regolith, the filaments need to be extruded twice by the single screw extruder, or using a more powerful

extrusion method, such as a twin-screw extruder. A smaller nozzle diameter, such as 0.4 mm, allows for printing with less material, which is critical in applications where material conservation is essential, and it enables the production of parts with finer details. However, it should be noted that printing with a 0.4 mm nozzle was not feasible for any composite filament due to clogging, except for SS2-10.

The 3D Benchy model, a widely recognized "torture test," was selected to further evaluate the printability of the filaments due to its complex geometry. As described in the definition of printability, the material's ability to maintain its shape during cooling to room temperature, bridge gaps, and produce fine details are critical characteristics of a printable material.

Fig. 6a and e displays the successfully printed parts using pure LDPE and composite filament containing 30 wt% regolith, respectively. The boat's wheel, a small, round, and intricate feature, highlights the filament's ability to produce fine details, which are well printed. The 3D Benchy model includes several gap-bridging features, such as multiple windows and portholes, which were successfully printed. A closer observation of the front window, which is the longest bridge in the part, shown in Fig. 6b and f, reveals that it is slouched, with the LDPE sample exhibiting more pronounced drooping than the composite sample. For a material to keep its shape without drooping, a high value of yield stress and a strong shear-thinning behaviour are required [48]. Previous studies have demonstrated that well-dispersed inorganic particles can introduce these properties to polymers [49,50].

Overhangs are among the most challenging aspects of 3D printing. The hull features a large overhanging curved surface, with a 40° spoon bow, which is critical and difficult to print, making it particularly revealing of surface deviations. As depicted in Fig. 6c, the overhang in the sample printed with pure LDPE is poorly formed and exhibits noticeable drooping. In contrast, the composite sample demonstrates a well printed overhang, with minor surface roughness (Fig. 6g). As Fig. 6d and h show, the 41° spoon bow in the composite sample more closely aligns with the CAD file compared to the 46° measurement observed in the LDPE sample. This increase in overhang dimensions beyond the CAD specifications is likely due to warpage.

To investigate the dimensional accuracy of the printed parts in greater detail, 3D Benchy models were scanned and aligned with their original CAD geometry. Fig. 7 presents the dimensional deviation results, highlighting differences between pure LDPE and LDPE/regolith composite. As shown in Fig. 7a, the PDF curve for the composite is narrower and more centered, indicating reduced variability and closer adherence to the nominal geometry. Quantitatively, the pure LDPE Benchy shows a mean deviation of −0.415 mm with a standard deviation of 0.668 mm, indicating a notable tendency to underbuilds. In contrast, the composite Benchy exhibits a smaller mean.

Deviation of −0.193 mm and a tighter spread (σ = 0.401 mm), reflecting improved dimensional consistency. The underbuilding observed in both cases is likely due to the shrinkage of LDPE during cooling, a behavior attributed to its relatively high crystallinity compared to typical FDM materials.

The surface deviation maps (Fig. 7b–e) further support these trends. While both materials exhibit localized overbuilding near the rear window and underbuilding at the bow and stern, the pure LDPE prints (Fig. 7b and c) show a broader spread of deviations. The composite prints (Fig. 7d and e) are predominantly green, indicating deviations within ±0.5 mm across most of the surface. Overall, the regolith-filled composite demonstrates reduced dimensional error and variability compared to the neat LDPE filament, confirming its suitability for FDM printing in terms of dimensional fidelity.

Fig. 8 shows the measured warpage values and the arc radius as a function of regolith wt% along with schematics of the printed parts. As illustrated, warpage decreases with increasing regolith wt% with nearly a half reduction (47 %) observed at 30 wt% regolith. These findings are aligned with previous studies demonstrating that the addition of fillers enhances dimensional stability by decreasing the part shrinkage and warpage [34,35].

Specific NASA components were printed using the composite material containing 30 wt% regolith. This approach enables a direct comparison to established benchmarks, demonstrating the potential of the developed composites for producing functional tools for future missions. Each component was designed to serve a specific purpose. For instance, the wire tie (Fig. 9a and b) was created to evaluate the material's flexibility. The results show that the composite retains a high degree of flexibility, a key property of LDPE, even at 30 wt% regolith loading. Additionally, the container (Fig. 9d and e) demonstrates the capability to print two interlocking parts simultaneously, with the threads of the container and lid fitting together securely. Furthermore, other functional tools, including a CubeSat clip (Fig. 9c), torque tool (Fig. 9f), and crowfoot (Fig. 9g), were successfully printed, highlighting the material's suitability for fabricating replacement tools in space environments.

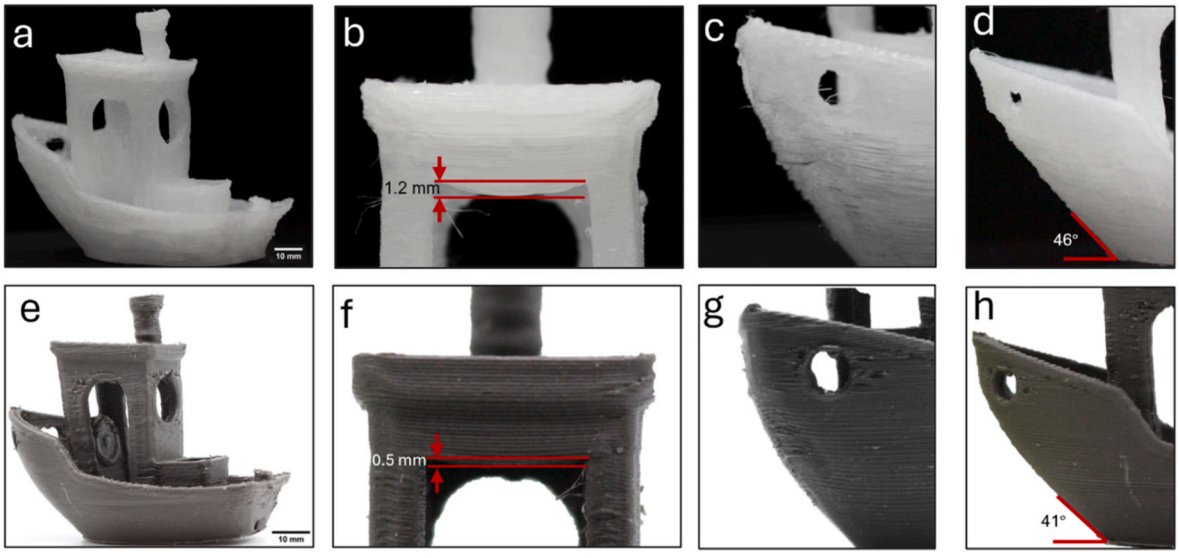

Fig. 6. Photographs of 3D Benchy printed with: a, c, e, g) pure LDPE; and b, d, f, h) 30 wt% regolith filaments. The model demonstrates the improved printability of the composite filament compared to pure LDPE.

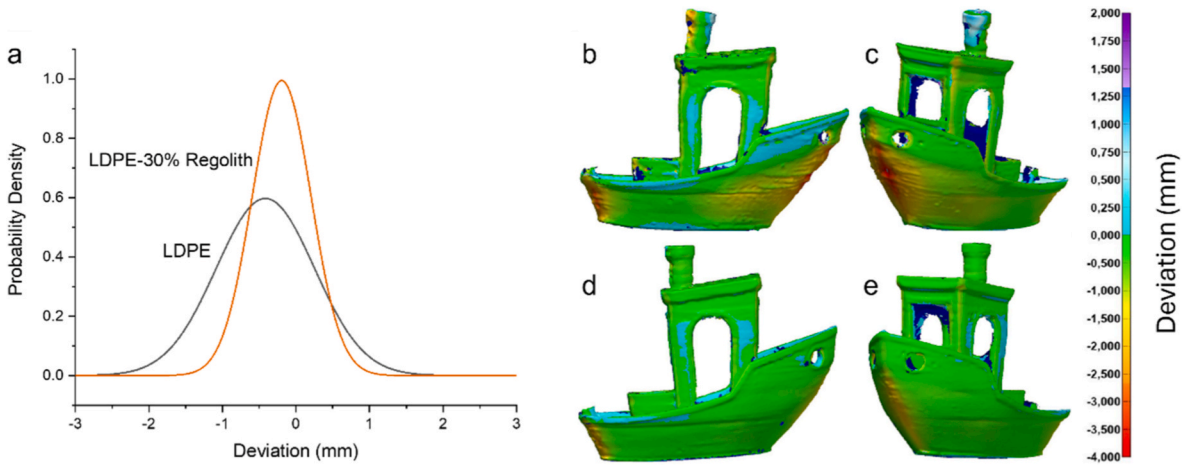

Fig. 7. Dimensional accuracy and geometric deviations of printed 3D Benchy compared to the CAD model: a) probability density curves; and surface deviation maps of printed parts using: b and c) pure LDPE; d and e) LDPE-30 wt% regolith filaments.

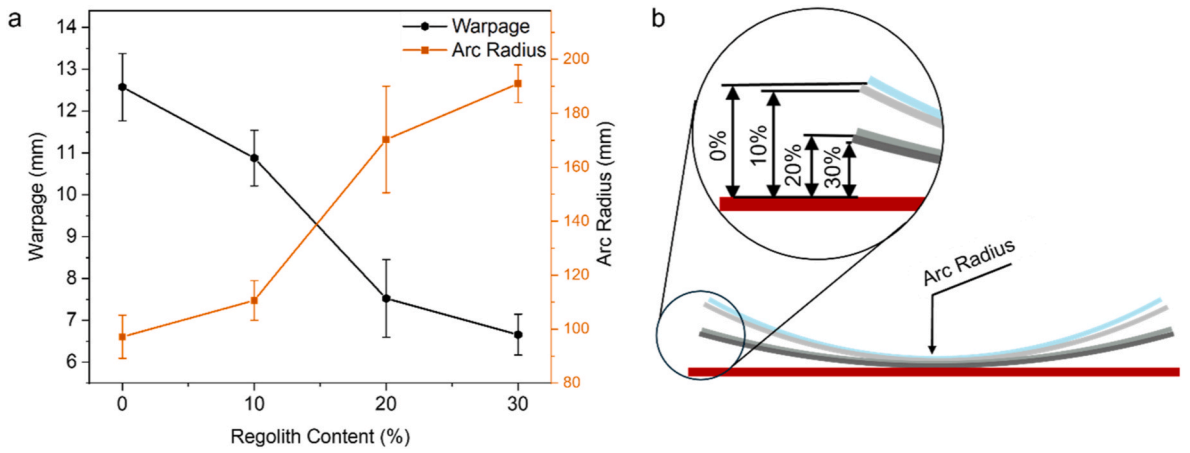

Fig. 8. Warpage and arc radius analysis of 3D printed rectangular cuboids (100 × 8 × 4 mm): a) the measured warpage values and the arc radius as a function of regolith wt%; and b) schematics of the warped printed samples.
Warpage decreases with increasing regolith content.

Though some of these parts, such as the container or wire tie, may not require demanding mechanical performance, others, such as the crowfoot or CubeSat clip, are more structurally critical. Therefore, the selection of actual engineering applications will ultimately depend on meeting mission specific requirements, which remain subject to further evaluation.

The successful 3D printing of both benchmark geometries and NASA-relevant tools using the composite filament containing up to 30 wt% regolith demonstrates that the developed material is printable and capable of producing dimensionally accurate components. This two stage validation approach; first confirming printability through commonly used benchmark geometries, then demonstrating applicability via functional tools, highlights the feedstock's potential for in-situ manufacturing and replacement parts in space and suggests significant potential for recycling applications and in-situ resource utilization for future lunar missions.

3.3. Tensile properties

Fig. 10 presents the tensile properties of the printed samples, and Table 3 summarizes the measured data. Representative stress–strain curves for each material are provided in Fig. 10a. For each material set, the representative curve was selected as the one closest to the average response of five tested replicates. All stress–strain curves demonstrate typical polymeric behavior characterized by an initial elastic deformation region followed by plastic deformation. As these curves do not show a point of zero slope, yield strength was calculated using the 0.2 % offset method.

Due to overlapping standard deviations in tensile strength values, ANOVA analysis was used to assess statistically significant differences among the samples. The analysis revealed that the addition of up to 20 wt% regolith did not significantly affect the tensile strength compared to pure LDPE. However, a reduction in tensile strength was observed at 30 wt% regolith compared to both pure LDPE and composites with lower regolith weight percentages. This behaviour aligns with findings from Azami et al. [17] at PEEK/30 wt% of regolith composites, as well as other studies on particulate-filled polymer composites at high weight fractions of micro-particles [18].

A reduction in tensile properties upon the addition of regolith is consistently reported in studies using the FFF 3D printing method, although the specific weight percentage at which this reduction occurs varies. Here, the reduction occurs at 30 wt%, whereas other studies reported it at lower content, such as 5 wt% and 10 wt% [15,17]. Direct comparisons between studies are challenging due to differences in the polymer matrix, regolith simulant properties (e.g., particle size distribution and shape), and processing/printing conditions. Nevertheless, we provide valuable insight, demonstrating that regolith can be incorporated into the polymer at up to 20 wt% without compromising tensile

Fig. 9. Photograph of 3D printed tools designed by NASA: a-b) wire tie; c) cube sat clip; d-e) container and lid with interlocking thread; f) crowfoot; and g) torque tool. All the parts are printed with composite containing 30 wt% regolith.
The image demonstrates the suitability of the composite for producing on-demand tools.

strength.

Several factors may contribute to the observed reduction in tensile strength at higher regolith content. First, in particle reinforced composite materials, the effective stress transfer between the polymeric matrix and filler particles is a critical factor influencing tensile strength. High filler content can lead to the formation of defects, such as particle agglomerations and porosity, which disrupt the microstructure's continuity and impair stress transfer, thereby reducing the material's strength. Previous studies have attributed the reduced tensile strength of lunar regolith composites to increased porosity compared to pure polymer [15,17].

Second, in 3D printed parts, the interlayer bonding strength plays a critical role in determining the mechanical properties. This strength is influenced by the degree of inter-molecular diffusion of polymer chains across the contact surfaces. At higher regolith content, less of the interlayer interface between adjacent deposited filaments is covered by polymer, as more surface area is occupied by regolith particles. Additionally, the presence of regolith may inhibit the inter-diffusion of polymer chains, potentially affecting interlayer bonding.

As shown in Fig. 10c, adding regolith increased stiffness by 13.8, 38, and 52 % at 10, 20, and 30 wt%, respectively. This enhancement is consistent with the well-known effect of incorporating inorganic particles into polymeric matrices, attributed to the higher stiffness of the rigid particles compared to the polymer matrix. Notably, the method of filament fabrication (twin screw extrusion vs. single screw extrusion) had negligible effect on both strength and stiffness, indicating that both methods are capable of producing materials with comparable properties.

Lastly, Fig. 10d presents yield strength results. In the presence of regolith, yield strength values remained generally similar to pure LDPE or slightly lower, particularly evident for the SS2-10 composite. A reduction in yield strength upon addition of microparticles to polymer matrices is commonly reported in literature Unlike tensile strength, which reflects the material's overall load-bearing capacity, yield stress is more sensitive to early-stage microstructural features. The yield behavior is dominated by local stress concentrations and filler agglomerates, often resulting in a non-linear decline as filler content increases [51,52]. Here, no clear or consistent trend was observed regarding the influence of regolith content or filament fabrication method on yield strength. Consequently, the available data do not support definitive conclusions about the isolated or combined effects of filler content and processing route on yield strength.

To better position our approach within the broader landscape of lunar additive manufacturing technologies, Table 4 presents a comparative summary of several promising AM technologies for in-situ lunar construction. Key parameters such as material, maximum regolith content, printing speed, current advantages and limitations are outlined for methods including solar light sintering (SLS), binder jetting (BJ), direct ink writing (DIW), stereolithography (SLA), vat photopolymerization (VP), alongside existing studies on FFF, to the best of our knowledge.

The FFF approach proposed in our work is unique by its integration of packaging grade LDPE, supporting both ISRU and waste management objectives. Although some binder-based techniques such as DIW or SLA have demonstrated higher regolith content (up to 80 wt%), they typically depend on Earth supplied binders and require energy intensive post processing like sintering. Here we use packaging grade LDPE, a common and potentially recyclable cargo material, as a binder, which is a resource-efficient alternative. This strategy enhances alignment with ISRU goals and introduces the possibility of managing plastic waste streams on the Moon. NASA's recent LunaRecycle Challenge estimates that nearly 100 kg of polyethylene waste could be generated during a one-year lunar mission involving eight crew members. While our current research uses virgin LDPE, the usage of actual packaging waste in future research is required to further close the resource loop.

Each AM technique summarized in Table 4 offers distinct trade-offs, and the selection of a method will depend on mission specific requirements. For instance, packaging waste may also be suited for FGF, although FGF is better suited for large scale manufacturing. With further optimization for higher regolith content and enhanced mechanical performance, FFF presents a promising, sustainable pathway for mission aligned manufacturing on the Moon.

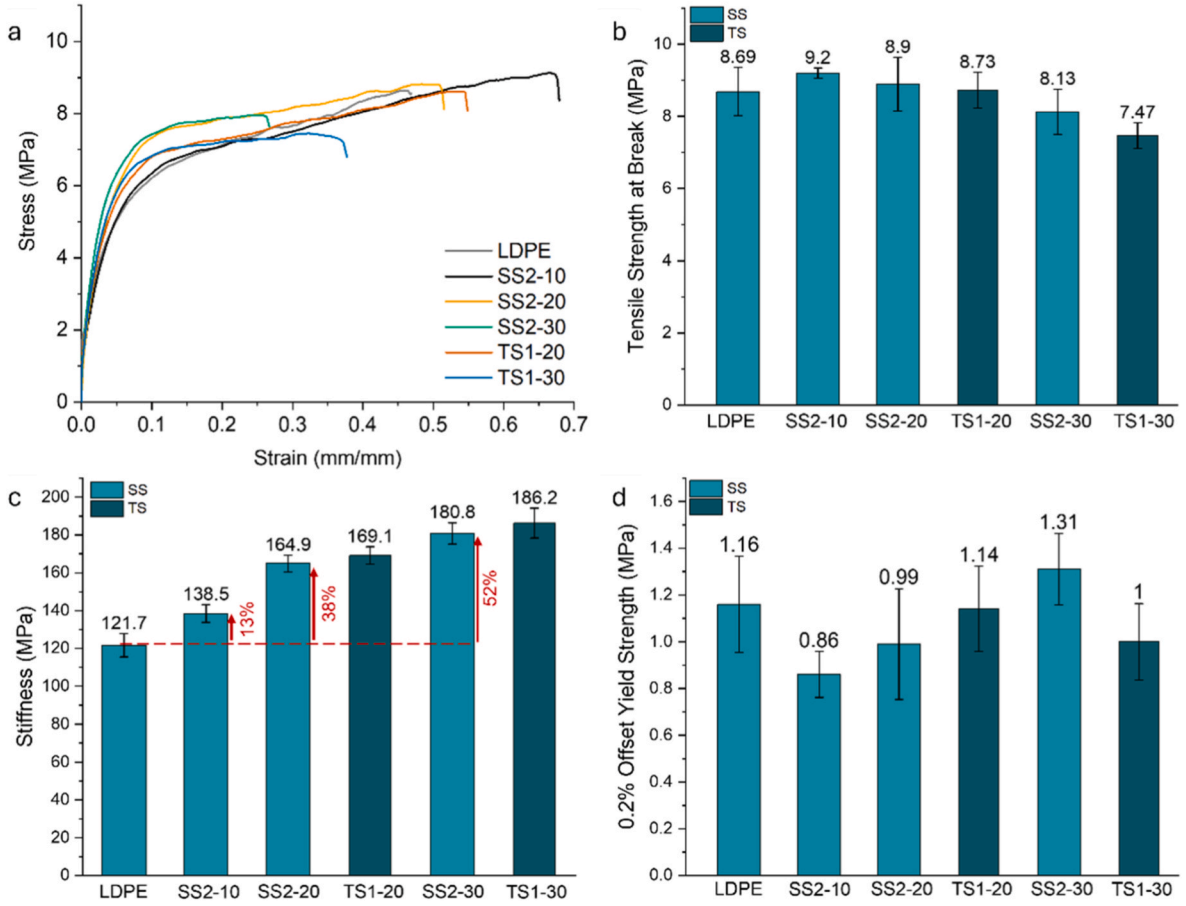

Fig. 10. Tensile mechanical properties of the 3D printed samples using filaments containing up to 30 wt% regolith fabricated by single-screw and twin-screw extrusion: a) stress-strain curves; b) tensile strength at break; c) stiffness; and d) 0.2 % offset yield strength.
Tensile strength decreases at 30 wt%, while stiffness increases with regolith content.

Table 3
Tensile properties of printed LDPE/regolith composite samples.

Sample	0.2 % Offset Yield Strength (MPa)	Tensile Strength at Break (MPa)	Stiffness (MPa)
LDPE	1.16 ± 0.20	8.69 ± 0.75	121.7 ± 6.2
SS2-10	0.85 ± 0.09	9.21 ± 0.16	138.5 ± 4.7
SS2-20	0.98 ± 0.23	8.91 ± 0.83	164.9 ± 4.4
SS2-30	1.31 ± 0.15	8.13 ± 0.70	180.8 ± 5.6
TS1-20	1.14 ± 0.18	8.74 ± 0.55	169.1 ± 4.6
TS1-30	0.99 ± 0.16	7.48 ± 0.40	186.2 ± 7.9

4. Conclusion

This study demonstrated the successful fabrication of 3D printable LDPE and LDPE/regolith composite filaments with up to 30 wt% regolith, using both a desktop single screw extruder and a twin-screw extruder. The results showed that a second extrusion step enhances processability at high regolith contents, enabling the production of printable filaments that single screw extrusion alone could not achieve above 10 wt%. This addresses the challenge of producing high regolith content filaments for ISRU applications.

The printability of the fabricated filaments was assessed by printing various components, including NASA-designed parts. The addition of regolith improved key 3D printing metrics such as overhang formation, gap bridging, and reduced warpage. Although here we used virgin packaging grade LDPE rather than the actual packaging waste, printing with two grades of packaging LDPE highlighted how a simple factor like MFI can play a crucial role in repurposing packaging materials for 3D printing. This underscores the importance of selecting the right polymer grade to enhance printability. While additives in packaging may influence properties, further research on post consumer waste is necessary to evaluate its full suitability for 3D printing.

Mechanical testing showed that regolith enhances stiffness without compromising tensile strength at up to 20 wt% regolith, although a reduction in strength was observed at 30 wt%. The fabrication method had no significant effect on mechanical properties, indicating that both single and twin screw extrusion can produce high quality filaments, albeit with distinct trade-offs. Single screw extrusion is more energy efficient and compact, making it advantageous for low resource environments like the Moon. In contrast, twin screw extrusion, though more energy intensive and complex, enhances processability at higher regolith contents, potentially reducing the usage of waste material and improving filament consistency. These trade-offs are critical for mission planning, influencing equipment selection, transport logistics, and overall sustainability in lunar manufacturing.

This research contributes to the development of recycling and ISRU strategies. Unlike other binder-based AM approaches, which often rely on Earth-supplied binders and require energy-intensive post-processing such as sintering, this FFF method uses packaging grade LDPE, a cargo material already present on lunar missions, as the binder. Implementing this method on the Moon would require a recycling line with an extrusion and printing system capable of processing thermoplastics and regolith composites, with energy demands varying based on extrusion type and heating requirements.

Our findings have significant implications for closing the material loop by converting polyethylene packaging waste into 3D printing

Table 4
Comparison of the current study with other FFF approaches and promising additive manufacturing methods for in space manufacturing.

AM method	Materials	Max regolith content	Printing Speed	Properties	Current advantages	Current limitations	Ref.
FFF	LDPE + lunar regolith	30 wt %	20 mm/s	Tensile Strength: 7.48 ± 0.40 MPa Stiffness: 186.2 ± 7.9 MPa	Uses only in-situ resources Supports packaging recycling	Requires further research on post consumer waste	Current study
	PEEK + lunar regolith	30 wt%	7.5 mm/s	Tensile strength: 67.0 MPa Young's modulus: 1152.1 MPa	High mechanical performance	Relies on polymer feedstock sourced from Earth	[17]
	MDPE + Martial regolith	10 wt%	20 mm/s	Tensile strength: 3.19 ± 0.70 MPa	Uses only in-situ resources	Requires further research on post consumer waste	[16]
	PLA + lunar regolith	10 wt%	80 mm/s	Tensile Strength: 53.0 ± 2.8 MPa	Recyclable printed parts	Relies on polymer feedstock sourced from Earth Potential outgassing of PLA	[15]
FGF	PLA + lunar regolith	80 wt%	12 Mm/s	Flexural modulus of 5.3 GPa and flexural strength of 24 MPa	Eliminates filament fabrication step Enables high printing speed	Relies on polymer feedstock sourced from Earth Potential outgassing of PLA	[53]
SLS	Regolith	–	30 mm/min	Compressive Strength: 4.25 MPa	Operates with direct solar energy input	Low strength Geometric inaccuracies	[54]
BJ	Binder + lunar regolith	–	–	Flexural strength: 66.95 ± 2.59 MPa	Potential for automation	Requires material supply from Earth Energy intensive post processing (sintering)	[55]
DIW	Ink + lunar regolith	74 vol%	5–6 mm/s	Peak compressive stress: 19 MPa Linear shrinkage: 10–15 %	High-resolution part fabrication	Requires material supply from Earth Energy intensive post processing (sintering)	[56]
SLA	Slurry + lunar regolith	80 wt%	–	Flexural strength: 132.21 MPa Compressive strength: 444.23 MPa	High-resolution part fabrication	Requires material supply from Earth Typically requires post processing via sintering	[57]
VP + sintering	Slurry + lunar regolith	65 wt%	–	Flexural strength: 106 ± 5 MPa Radial and linear shrinkage: 20 ± 5 %	High-resolution part fabrication	Requires material supply from Earth Energy intensive post processing (sintering)	[58]

feedstock for lunar applications. This approach supports resource efficiency and circular economy principles for long duration lunar missions. The results demonstrated the potential of LDPE/regolith composites for manufacturing essential tools and replacement parts directly on the Moon, reducing feedstock transportation costs and dependence on Earth-based resupply. By integrating this method into future ISRU and waste management strategies, lunar habitats could become more self sufficient, paving the way to support long term human presence beyond Earth.

CRediT authorship contribution statement

S. Moazen: Writing – original draft, Methodology, Investigation, Formal analysis. **F.P. Gosselin:** Writing – review & editing, Supervision, Methodology. **I. Tabiai:** Writing – review & editing, Supervision, Methodology. **M. Dubé:** Writing – review & editing, Supervision, Methodology, Funding acquisition, Conceptualization.

Declaration of competing interest

The authors declare that they have no known competing financial interests or personal relationships that could have appeared to influence the work reported in this paper.

Acknowledgements

This work was funded by CREPEC (Research Center for High Performance Polymer and Composites). A special thanks to Dr. Marie-Josée Potvin from the Canadian Space Agency for her consultations and support. We would also like to acknowledge Dr. Melanie Girard for her participation in the early stages of the project, and Emma July, our intern for her assistance with preliminary 3D printing testing.

Appendix A. Supplementary data

Supplementary data to this article can be found online at https://doi.org/10.1016/j.actaastro.2025.08.012.

References

[1] M.J. Werkheiser, M. Fiske, J. Edmunson, B. Khoshnevis, On the development of additive construction technologies for application to development of lunar/martian surface structures using in-situ materials, in: AIAA SPACE 2015 Conf. Expo, American Institute of Aeronautics and Astronautics, 2015, https://doi.org/10.2514/6.2015-4451.
[2] T.J. Prater, M.J. Werkheiser, A. Jehle, F. Ledbetter, Q. Bean, M. Wilkerson, et al., NASA's in-space manufacturing project: development of a multimaterial fabrication Laboratory for the International space station, in: AIAA SPACE Astronaut. Forum Expo, American Institute of Aeronautics and Astronautics, 2017, https://doi.org/10.2514/6.2017-5277.
[3] D.L. Linne, B.A. Palaszewski, S.A. Gokoglu, B. Balasubramaniam, U.G. Hegde, C. Gallo, Waste management Options for long-duration space missions: when to Reject, Reuse, or recycle, in: 7th Symp. Space Resour. Util., American Institute of Aeronautics and Astronautics, 2014, https://doi.org/10.2514/6.2014-0497.
[4] M. Hoffmann, A. Elwany, In-space additive manufacturing: a review, J. Manuf. Sci. Eng. 145 (2022), https://doi.org/10.1115/1.4055603.
[5] A.A. Altun, F. Ertl, M. Marechal, A. Makaya, A. Sgambati, M. Schwentenwein, Additive manufacturing of lunar regolith structures, Open Ceram 5 (2021) 100058, https://doi.org/10.1016/j.oceram.2021.100058.
[6] M. Azami, Z. Kazemi, S. Moazen, M. Dubé, M.-J. Potvin, K. Skonieczny, A comprehensive review of lunar-based manufacturing and construction, Prog. Aero. Sci. 150 (2024) 101045, https://doi.org/10.1016/j.paerosci.2024.101045.
[7] M. Isachenkov, S. Chugunov, I. Akhatov, I. Shishkovsky, Regolith-based additive manufacturing for sustainable development of lunar infrastructure – an overview, Acta Astronaut. 180 (2021) 650–678, https://doi.org/10.1016/j.actaastro.2021.01.005.
[8] M.S. Suhaizan, P. Tran, A. Exner, B.G. Falzon, Regolith sintering and 3D printing for lunar construction: an extensive review on recent progress, Prog Addit Manuf 9 (2024) 1715–1736, https://doi.org/10.1007/s40964-023-00537-1.
[9] M. Isachenkov, I. Gorokh, E. Makarov, D. Verkhoturov, P. Khmelenko, N. Garzaniti, et al., Technical evaluation of additive manufacturing technologies for in-situ fabrication with lunar regolith, Adv. Space Res. 71 (2023) 2656–2668, https://doi.org/10.1016/j.asr.2022.07.075.

[10] P. Zhang, W. Dai, R. Niu, G. Zhang, G. Liu, X. Liu, et al., Overview of the lunar in situ resource utilization techniques for future lunar missions, Space Sci Technol 3 (2023) 37, https://doi.org/10.34133/space.0037.
[11] Redwire's Ceramic Manufacturing Module Successfully 3D Prints Turbine Blisk In Space, Manufactur3D (2020). https://manufactur3dmag.com/redwires-ceramic-manufacturing-module-successfully-3d-prints-turbine-blisk-in-space/. (Accessed 1 July 2025).
[12] ESA launches first metal 3D printer to ISS n.d. https://www.esa.int/Science_Exploration/Human_and_Robotic_Exploration/ESA_launches_first_metal_3D_printer_to_ISS (accessed July 1, 2025).
[13] T. Prater, N. Werkheiser, F. Ledbetter, K. Morgan, In-space manufacturing at NASA Marshall space Flight center: a Portfolio of fabrication and recycling technology development for the International space station. https://directory.eoportal.org/web/eoportal/satellite-missions/i/iss-refabricator, 2018. (Accessed 30 May 2022).
[14] T. Prater, N. Werkheiser, F. Ledbetter, D. Timucin, K. Wheeler, M. Snyder, 3D Printing in Zero G Technology Demonstration Mission: complete experimental results and summary of related material modeling efforts, Int. J. Adv. Manuf. Technol. 101 (2019) 391–417, https://doi.org/10.1007/s00170-018-2827-7.
[15] H. Li, W. Zhao, X. Wu, H. Tang, Q. Li, J. Tan, et al., 3D printing and Solvent Dissolution recycling of Polylactide–lunar regolith composites by material extrusion approach, Polymers 12 (2020) 1724, https://doi.org/10.3390/polym12081724.
[16] F. Zaccardi, E. Toto, M.G. Santonicola, S. Laurenzi, 3D printing of radiation shielding polyethylene composites filled with Martian regolith simulant using fused filament fabrication, Acta Astronaut. 190 (2022) 1–13, https://doi.org/10.1016/j.actaastro.2021.09.040.
[17] M. Azami, P.-L. Aubin-Fournier, K. Skonieczny, Enhancing economical lunar-based manufacturing by incorporating lunar regolith into polyether–ether–ketone (PEEK): material development, additive manufacturing, and characterization, Prog Addit Manuf (2025), https://doi.org/10.1007/s40964-024-00934-0.
[18] N.J. Gelino, JacksonL. Smith, T.D. Irwin, T.A. Lipscomb, E.A. Bell, D.I. Malott, et al., Selection, production, and properties of regolith polymer composites for lunar construction, in: 2024 IEEE Aerosp. Conf., Big Sky, IEEE, MT, USA, 2024, pp. 1–21, https://doi.org/10.1109/AERO58975.2024.10521133.
[19] W.A. Campbell, J.J. Scialdone, Outgassing Data for Selecting Spacecraft Materials, 1993.
[20] M. Perchonok, NASA, We Have a Challenge and It's Food Packaging, 2014.
[21] I. Sakurada, K. Kaji, S. Wadano, Elastic moduli and structure of low density polyethylene, Colloid Polym. Sci. 259 (1981) 1208–1213, https://doi.org/10.1007/BF01525016.
[22] J.R.V. Wazer, Viscosity and Flow Measurement: A Laboratory Handbook of Rheology, Interscience Publishers, 1963.
[23] H.A. Barnes, J.F. Hutton, K. Walters (Eds.), Rheology Series. Rheol. Ser., 3, Elsevier, 1989, p. ii, https://doi.org/10.1016/B978-0-444-87469-6.50001-9.
[24] E.L. Gilmer, D. Miller, C.A. Chatham, C. Zawaski, J.J. Fallon, A. Pekkanen, et al., Model analysis of feedstock behavior in fused filament fabrication: enabling rapid materials screening, Polymer 152 (2018) 51–61, https://doi.org/10.1016/j.polymer.2017.11.068.
[25] P. Olesik, M. Godzierz, M. Kozioł, Preliminary characterization of Novel LDPE-based Wear-Resistant composite suitable for FDM 3D printing, Materials 12 (2019) 2520, https://doi.org/10.3390/ma12162520.
[26] K.R. Hart, J.B. Frketic, J.R. Brown, Recycling meal-ready-to-eat (MRE) pouches into polymer filament for material extrusion additive manufacturing, Addit. Manuf. 21 (2018) 536–543, https://doi.org/10.1016/j.addma.2018.04.011.
[27] N. Venkataraman, S. Rangarajan, M.J. Matthewson, B. Harper, A. Safari, S. C. Danforth, et al., Feedstock material property – process relationships in fused deposition of ceramics (FDC), Rapid Prototyp. J. 6 (2000) 244–253, https://doi.org/10.1108/13552540010373344.
[28] M. Hassanien, Evaluation and improvement of mechanical, thermal and rheological properties of polypropylene (PP) using linear low density polyethylene (LLDPE), Int J Eng Sci Innov Technol IJESIT 3 (2014) 55–60.
[29] P. Bedi, R. Singh, I. Ahuja, Effect of SiC/Al2O3 particle size reinforcement in recycled LDPE matrix on mechanical properties of FDM feed stock filament, Virtual Phys. Prototyp. 13 (2018) 246–254, https://doi.org/10.1080/17452759.2018.1496605.
[30] S. Wang, L. Capoen, D.R. D'hooge, L. Cardon, Can the melt flow index be used to predict the success of fused deposition modelling of commercial poly(lactic acid) filaments into 3D printed materials? Plast, Rubber Compos. 47 (2018) 9–16, https://doi.org/10.1080/14658011.2017.1397308.
[31] F. Peng, H. Jiang, A. Woods, P. Joo, E.J. Amis, N.S. Zacharia, et al., 3D printing with Core–Shell filaments containing high or low density polyethylene Shells, ACS Appl. Polym. Mater. 1 (2019) 275–285, https://doi.org/10.1021/acsapm.8b00186.
[32] C.G. Schirmeister, T. Hees, E.H. Licht, R. Mülhaupt, 3D printing of high density polyethylene by fused filament fabrication, Addit. Manuf. 28 (2019) 152–159, https://doi.org/10.1016/j.addma.2019.05.003.
[33] P. Jeyachandran, S. Bontha, S. Bodhak, V.K. Balla, B. Kundu, M. Doddamani, Mechanical behaviour of additively manufactured bioactive glass/high density polyethylene composites, J. Mech. Behav. Biomed. Mater. 108 (2020) 103830, https://doi.org/10.1016/j.jmbbm.2020.103830.
[34] P. Beesetty, A. kale, B. Patil, M. Doddamani, Mechanical behavior of additively manufactured nanoclay/HDPE nanocomposites, Compos. Struct. 247 (2020) 112442, https://doi.org/10.1016/j.compstruct.2020.112442.
[35] A. Gudadhe, N. Bachhar, A. Kumar, P. Andrade, G. Kumaraswamy, Three-dimensional printing with waste high-density polyethylene, ACS Appl. Polym. Mater. 1 (2019) 3157–3164, https://doi.org/10.1021/acsapm.9b00813.
[36] M. Spoerk, F. Arbeiter, I. Raguž, G. Weingrill, T. Fischinger, G. Traxler, et al., Polypropylene filled with glass Spheres in extrusion-based additive manufacturing: effect of filler size and printing Chamber temperature, Macromol. Mater. Eng. 303 (2018) 1800179, https://doi.org/10.1002/mame.201800179.
[37] R. Singh, P. Bedi, F. Fraternali, I.P.S. Ahuja, Effect of single particle size, double particle size and triple particle size Al2O3 in Nylon-6 matrix on mechanical properties of feed stock filament for FDM, Composites, Part B 106 (2016) 20–27, https://doi.org/10.1016/j.compositesb.2016.08.039.
[38] A.M. Abdullah, T.N.A. Tuan Rahim, D. Mohamad, H.M. Akil, Z.A. Rajion, Mechanical and physical properties of highly ZrO2/β-TCP filled polyamide 12 prepared via fused deposition modelling (FDM) 3D printer for potential craniofacial reconstruction application, Mater. Lett. 189 (2017) 307–309, https://doi.org/10.1016/j.matlet.2016.11.052.
[39] P. Awasthi, S.S. Banerjee, Fused deposition modeling of thermoplastic elastomeric materials: challenges and opportunities, Addit. Manuf. 46 (2021) 102177, https://doi.org/10.1016/j.addma.2021.102177.
[40] W. Kanabenja, N. Passornraprasit, C. Aumnate, T.A. Osswald, D. Aht-Ong, P. Potiyaraj, Enhancing 3D printability of polyhydroxybutyrate (PHB) and poly(3-hydroxybutyrate-co-3-hydroxy valerate) (PHBV) based blends through melt extrusion based-3D printing, Addit. Manuf. 86 (2024) 104205, https://doi.org/10.1016/j.addma.2024.104205.
[41] M. Parker, A. Inthavong, E. Law, S. Waddell, N. Ezeokeke, R. Matsuzaki, et al., 3D printing of continuous carbon fiber reinforced polyphenylene sulfide: Exploring printability and importance of fiber volume fraction, Addit. Manuf. 54 (2022) 102763, https://doi.org/10.1016/j.addma.2022.102763.
[42] C. Duty, C. Ajinjeru, V. Kishore, B. Compton, N. Hmeidat, X. Chen, et al., What makes a material printable? A viscoelastic model for extrusion-based 3D printing of polymers, J. Manuf. Process. 35 (2018) 526–537, https://doi.org/10.1016/j.jmapro.2018.08.008.
[43] C.E. Zawaski, E.M. Wilts, C.A. Chatham, A.T. Stevenson, A.M. Pekkanen, C. Li, et al., Tuning the material properties of a water-soluble ionic polymer using different counterions for material extrusion additive manufacturing, Polymer 176 (2019) 283–292, https://doi.org/10.1016/j.polymer.2019.06.005.
[44] C.A. Chatham, C.E. Zawaski, D.C. Bobbitt, R.B. Moore, T.E. Long, C.B. Williams, Semi-crystalline polymer blends for material extrusion additive manufacturing printability: a case study with poly(ethylene terephthalate) and polypropylene, Macromol. Mater. Eng. 304 (2019) 1800764, https://doi.org/10.1002/mame.201800764.
[45] Q.A. Bean, K.G. Cooper, J.E. Edmunson, M.M. Johnston, M.J. Werkheiser, International Space Station (ISS) 3D Printer Performance and Material Characterization Methodology, Washington, DC, United States, 2015.
[46] Models | 3D Resources n.d. https://nasa3d.arc.nasa.gov/models/printable (accessed February 19, 2025).
[47] C. Cardona, A. Curdes, A. Isaacs, Effects of filament diameter tolerances in fused filament fabrication, IU J Undergrad Res 2 (2016) 44–47, https://doi.org/10.14434/iujur.v2i1.20917.
[48] A.J. Poslinski, M.E. Ryan, R.K. Gupta, Rheological behavior of filled polymeric systems I. Yield stress and shear-thinning effects, J. Rheol. 32 (1988) 703–735, https://doi.org/10.1122/1.549987.
[49] M. Bertolino, D. Battegazzore, R. Arrigo, A. Frache, Designing 3D printable polypropylene: material and process optimisation through rheology, Addit. Manuf. 40 (2021) 101944, https://doi.org/10.1016/j.addma.2021.101944.
[50] R.K. Gupta, Polymer and Composite Rheology, second ed., CRC Press, Boca Raton, 2000 https://doi.org/10.1201/9781482273700.
[51] B. Pukanszky, Effect of interfacial interactions on the deformation and failure properties of PP/CaCO3 composites, New Polym. Mater. 3 (1992) 205–217.
[52] M.A. Osman, J.E.P. Rupp, U.W. Suter, Tensile properties of polyethylene-layered silicate nanocomposites, Polymer 46 (2005) 1653–1660, https://doi.org/10.1016/j.polymer.2004.11.112.
[53] N.J. Gelino, E.A. Bell, D.I. Malott, S.E. Pfund, M.W. Nugent, M.A. Gudino, Application of regolith polymer composite fused granular fabrication construction in Simulated lunar conditions, in: Earth Space 2024, American Society of Civil Engineers, Miami, Florida, 2024, pp. 844–857, https://doi.org/10.1061/9780784485736.075.
[54] H. Yang, H. Wang, B. Xie, M. Sun, S. Chen, Z. Zhang, et al., Feasibility study and prospects analysis of lunar regolith forming based on concentrated solar energy, Acta Astronaut. 232 (2025) 424–438, https://doi.org/10.1016/j.actaastro.2025.03.031.
[55] M. Mariani, F. Bertolini, M. Isachenkov, C. Galassi, N. Lecis, A. Grande, et al., Binder Jetting of Lunar Regolith: 3D Printing and Densification, 2024, pp. 1–8.
[56] S.L. Taylor, A.E. Jakus, K.D. Koube, A.J. Ibeh, N.R. Geisendorfer, R.N. Shah, et al., Sintering of micro-trusses created by extrusion-3D-printing of lunar regolith inks, Acta Astronaut. 143 (2018) 1–8, https://doi.org/10.1016/j.actaastro.2017.11.005.
[57] C. Xiao, K. Zheng, S. Chen, N. Li, X. Shang, F. Wang, et al., Additive manufacturing of high solid content lunar regolith simulant paste based on vat photopolymerization and the effect of water addition on paste retention properties, Addit. Manuf. 71 (2023) 103607.
[58] M. Isachenkov, A.M. Grande, G. Sala, Optimizing lunar regolith for vat polymerization and sintering: pre-processing & mineral composition impact, Ceram. Int. 50 (2024) 32265–32277, https://doi.org/10.1016/j.ceramint.2024.06.034.